

CONCEPTUAL ARCHETYPE DECOMPOSITION FOR INTERPRETABLE AND GENERALIZABLE MODEL DECISIONS

Anonymous authors

Paper under double-blind review

ABSTRACT

Traditional concept decomposition methods have made significant progress in improving the interpretability of deep learning models, but they still face many challenges. A key issue is that they often lack traceable explanations for concepts, making it difficult to understand and verify how models make decisions and provide explanations based on specific concepts. To overcome this limitation, this paper proposes a new method—Conceptual Archetype Decomposition (CAD)—which aims to provide more interpretable concept learning and decision-making process. Unlike existing methods, our approach ensures that each concept can be represented as a linear combination of training samples, with its total activation value equal to 1. This constraint limits the learning space of the concepts and enhances their interpretability. Therefore, the advantage of our method lies in its fine-grained concept activation decomposition, which directly constructs the explanatory space between training samples and concepts. Through a dual-index decision mechanism, we deeply analyze the relationship between test samples and training samples. Extensive experiments on the CUB and ImageNet datasets demonstrate that our model not only improves decision transparency but also exhibits stronger generalization ability in multi-class classification tasks. Our code is available at: <https://anonymous.4open.science/r/CAD-4510/>.

1 INTRODUCTION

In recent years, the increasing reliance on deep learning models in high-risk domains such as healthcare and autonomous driving has highlighted the urgent need for model interpretability (Wang & Chung, 2022; Corfmat et al., 2025). While these models have achieved impressive performance, their opacity poses a significant challenge to understanding the decision-making process (Ribeiro et al., 2016; Selvaraju et al., 2017), which is crucial for ensuring their reliability and safety. Specifically, the lack of clear explanations for the features or concepts driving model predictions often undermines the interpretability of the decision-making process. This issue has sparked a wave of research on explainable deep learning models, particularly those based on concepts (Kim et al., 2018; Lee et al., 2024), aiming to extract human-understandable features from complex models.

A promising approach in this area is Concept Recursive Activation Factorization (CRAFT) (Fel et al., 2023), which decomposes the activations of neural network intermediate layers into a set of concept vectors and their corresponding coefficients via Non-Negative Matrix Factorization (NMF) (Lee & Seung, 1999). Although CRAFT provides a framework for identifying latent concepts in the decision process, it suffers from two key limitations: (i) the extracted concepts lack clear interpretability; (ii) it is difficult to establish an effective link between test samples and training samples in the decision process. Specifically, the concept vectors extracted by CRAFT lack clear semantic meaning, making it challenging to directly map them to interpretable features, and as a result, understanding the specific meaning of each concept becomes difficult. Additionally, the relationship between the concepts in CRAFT and the input data is not well-defined, affecting the model’s robustness and generalization capabilities.

To overcome these limitations, we propose a novel framework—Concept Archetype Decomposition (CAD)—designed to enhance the interpretability and robustness of concept-based deep learning models. Unlike previous methods such as CRAFT, CAD modifies the standard matrix factorization approach by representing the concept extraction process as a linear combination of the activation matrix A and two additional matrices: the concept index matrix C and the concept reconstruction matrix B . This method ensures that each concept is associated with specific training samples during the training process and is formed

054 through their linear combination, thus avoiding the issue in CRAFT where there is no direct connection
 055 between the activation matrix and concept vectors, leading to clearer semantic meanings for each concept.
 056

057 CAD satisfies a nested bilayer convex combination, meaning that each reconstruction can be fully indexed
 058 without encountering the issue in CRAFT where some samples cannot be explained. Additionally, CAD
 059 inherently adopts a Low-Entropy Structure, which avoids the influence of hyperparameters when setting
 060 regularization loss functions (Zhu et al., 2024). This allows for direct sparse results, thereby mitigating the
 061 impact of hyperparameter randomness on the concept decomposition.

062 During the testing phase, CAD uses the same weight matrix C learned during training to optimize and obtain
 063 the concept reconstruction matrix for the test samples, thus enabling the decomposition of new samples into
 064 concepts. Extensive experiments on benchmark datasets such as CUB (Wah et al., 2011) and ImageNet
 065 demonstrate (Deng et al., 2009) that our method not only enhances decision transparency but also exhibits
 066 stronger generalization capabilities. The main contributions of this paper are summarized as follows:

- 067 • We propose Concept Archetype Decomposition (CAD), a novel concept extraction method that
 068 avoids the distributional mismatch issue present in CRAFT decomposition (Fel et al., 2023), while
 069 also ensuring full interpretability, meaning that the concept vectors themselves are interpretable and
 070 indexable.
- 071 • The CAD design satisfies a nested bilayer convex combination and inherently adopts a Low-Entropy
 072 Structure, which helps avoid the influence of hyperparameter randomness in concept decomposition.
- 073 • We demonstrate the effectiveness of CAD on benchmark datasets, showing that it outperforms
 074 existing methods in both interpretability and robustness. We also provide a fully open-source code
 075 package for community research.

077 2 RELATED WORK

078 2.1 TRADITIONAL INTERPRETABILITY METHODS

079 There are two main directions in the field of interpretability research: one is Post-hoc interpretability,
 080 represented by works such as Grad-CAM (Selvaraju et al., 2017), IG (Sundararajan et al., 2017), Shapley
 081 (Lundberg & Lee, 2017), and LIME (Ribeiro et al., 2016). The other is the construction of inherently
 082 interpretable models, such as Concept Bottleneck Models (CBMs) (Koh et al., 2020). In most cases, Post-
 083 hoc methods are more valuable because there has already been a significant body of work that performs
 084 exceptionally well, and we only need to provide reasonable explanations for their behavior. On the other
 085 hand, inherently interpretable models are subject to the limitation of being "inherently interpretable," which
 086 may result in slightly inferior performance compared to models without such constraints.

087 In this paper, we focus on Post-hoc methods. Existing research, such as Grad-CAM (Selvaraju et al., 2017),
 088 IG, and other more advanced attribution methods (Zhu et al., 2024), aims to construct a heatmap to help
 089 humans understand which regions are important and what features the model relies on for decision-making.
 090 However, the issue with these methods is that they only highlight important regions but fail to explain what
 091 is within those regions, specifically what factors contribute to the prediction outcome.

092 2.2 RESEARCH AND APPLICATION OF CONCEPT DECOMPOSITION EXPLAINABILITY

093 In recent years, several concept-based decomposition methods have been introduced to address the issue of
 094 explaining decision-making criteria. A substantial body of research has demonstrated the applications of
 095 concept decomposition in interpretability. For instance, methods like Representational Similarity Via Inter-
 096 pretative Visual Concepts (RSVC) (Kondapaneni et al., 2025) and Representational Difference Explanations
 097 (RDX) (Kondapaneni et al., 2025) use concept decomposition results to study differences between models.
 098 ModelDiff (Shah et al., 2023) leverages this technique to investigate the impact of different training strategies,
 099 making the study of concept decomposition interpretability highly valuable. A representative method, Test-
 100 ing With Concept Activation Vectors (TCAV) (Kim et al., 2018), allows users to provide datasets with and
 101 without a specific concept, from which it learns a concept vector to decompose the corresponding concept.
 102 This approach also enables observation of factors present in an unseen dataset through concept matching.
 103 However, this method relies on manually provided concept sets, making it unsuitable in cases where the
 104 data is complex or the number of concepts is large. Additionally, since concept selection depends on human
 105 expertise, it faces the challenge of missing important concepts due to incomplete concept sets.

108 CRAFT (Fel et al., 2023), another concept extraction method, utilizes non-negative matrix factorization
 109 to decompose intermediate feature vectors (Lee & Seung, 1999). However, its training distribution and
 110 decomposition distribution are inconsistent, leading to the introduction of many out-of-distribution concepts
 111 during decomposition. Furthermore, CRAFT requires feature vectors to be strictly positive, making it
 112 unsuitable for models that do not meet this condition.

113 The core issue with the above decomposition methods lies in the fact that the concept vectors are learned,
 114 and obtaining interpretability for these concept vectors is inherently difficult. In other words, while we can
 115 decompose concepts, we cannot be certain of what those concepts represent. The proposed CAD method
 116 leverages convex properties to ensure that each concept can be indexed to its corresponding samples, thereby
 117 providing full interpretability. We ensure that every sample’s decomposition can necessarily lead to its
 118 concept composition, and each concept is directly associated with the corresponding sample explanation.

120 3 METHOD

122 In this paper, we propose a novel framework, Conceptual Archetype Decomposition (CAD), aimed at en-
 123 hancing the interpretability and robustness of concepts in concept-based interpretable deep learning models.
 124 Compared to previous methods such as CRAFT (Fel et al., 2023), our approach addresses two key issues: (i)
 125 the lack of intrinsic explanations for the extracted individual concepts, and (ii) the challenge of establishing
 126 associations between test and training samples during the model’s decision-making process. The following
 127 sections will present our method in detail, organized into three subsections: Problem Definition, Preliminary,
 128 and Conceptual Archetype Decomposition.

130 3.1 PROBLEM DEFINITION

132 Given a training sample $x^{(i)} \in \mathbb{R}^{w \times h \times 3}$ (where 3 corresponds to the image’s RGB channels, and h and w
 133 are the image’s height and width, respectively) and its corresponding class label $y^{(i)}$, we aim to design a
 134 method that decomposes the feature representations of deep neural networks into human-understandable
 135 concepts. Traditional methods for concept decomposition typically rely on subregion cropping (?), where
 136 the original training sample $x^{(i)}$ is cropped into a patch $x'^{(i)} \in \mathbb{R}^{c \times s \times s}$ of length and width $s \times s$. However,
 137 this approach often results in a shift in the input distribution between model training and testing, increasing
 138 the risk of reduced interpretability and robustness of the extracted concepts. This is because the model was
 139 not trained on these samples during training, which means that their distribution differs significantly from
 140 that of the training set. We train the model by feeding the entire image into the input, ensuring consistent
 141 inputs between training and inference. Next, we use a mapping function g that maps the full-image input
 142 $x^{(i)} \in \mathbb{R}^{w \times h \times 3}$ to an intermediate state $A(x^{(i)}) \in \mathbb{R}^{w \times h \times c}$ for decomposition (Goodfellow et al., 2016).
 143 Finally, the classifier h maps the intermediate state to the output, ensuring $f(x^{(i)}) = h(g(x^{(i)}))$. At this
 144 point, $f : x^{(i)} \rightarrow y^{(i)}$.

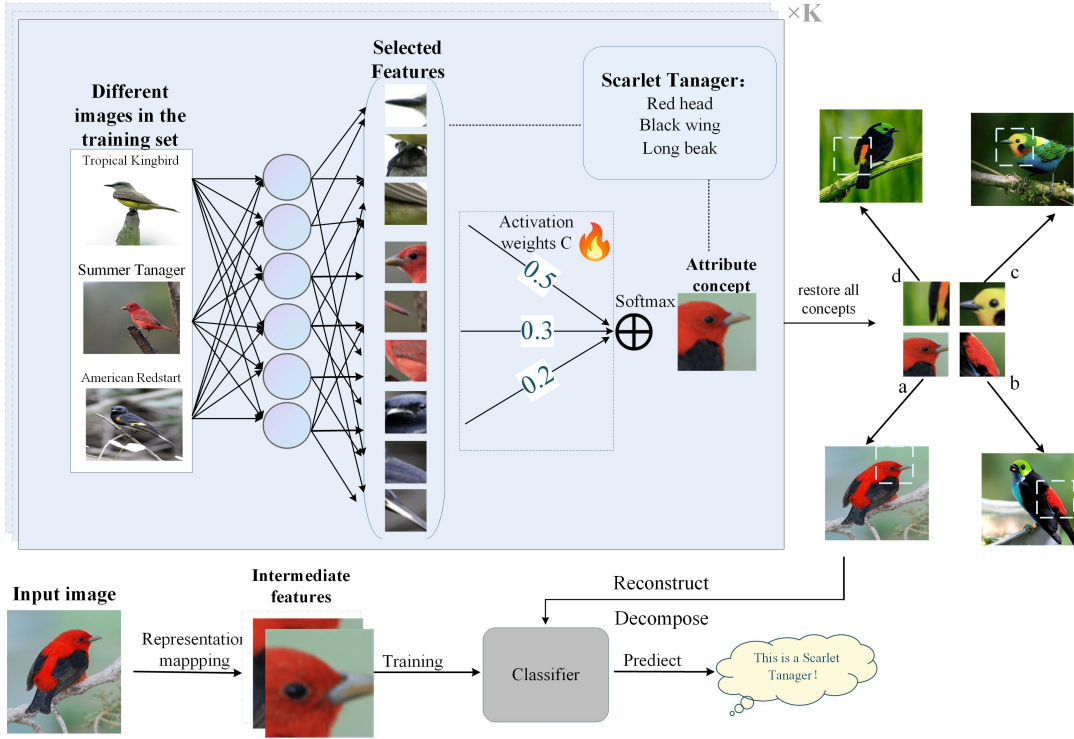
145 3.2 PRELIMINARIES

147 To enhance the interpretability of deep neural network models, the CRAFT method (Fel et al., 2023)
 148 employs Non-negative Matrix Factorization (NMF) techniques (Lee & Seung, 1999). NMF is an algorithm
 149 that decomposes a non-negative data matrix into two non-negative matrices, with each matrix representing
 150 different feature dimensions of the data. In CRAFT, NMF is used to factorize the activation matrix from
 151 the intermediate layers of the neural network into two matrices, which represent the concept dictionary and
 152 the concept coefficients, respectively. In this way, CRAFT is able to identify and extract the latent concepts
 153 involved in the decision-making process of the neural network, thereby aiding in the understanding of how
 154 the network reasons from input to output. The objective of NMF, in this context, is to minimize the following
 155 optimization problem:

$$156 \hat{U}, \hat{W} = \min_{U, W} \|A - UW^\top\|_F^2, \quad \text{if and only if } U, W \geq 0 \quad (1)$$

159 First, we need to reshape the matrix so that $A \in \mathbb{R}^{nwh \times c}$ represents the activation matrix extracted from
 160 the intermediate layer of the neural network, used to represent the sample. n is the number of samples,
 161 and $wh \times c$ is the feature dimension of each sample. $W \in \mathbb{R}^{k \times c}$ represents the concept dictionary matrix,
 which provides the concept activation vector. $U \in \mathbb{R}^{nwh \times k}$ is the concept coefficient matrix, which contains

162 the representation of each sample based on these concepts. k represents the number of extracted concepts.
 163 Furthermore, CRAFT’s (Fel et al., 2023) reconstruction process is $A \approx UW$. Therefore, U and W do not
 164 establish a direct connection with the activation A , making it difficult to extract the inherent meaning of
 165 the concepts. In other words, even if we obtain the final optimized concept matrix \hat{W} , we cannot accurately
 166 deconstruct it and cannot fully understand the meaning of each concept.
 167
 168
 169



194 Figure 1: The overall architecture of our proposed Conceptual Archetype Decomposition (CAD) method.
 195 The process includes feature extraction from an input image, followed by decomposition and reconstruction,
 196 ultimately leading to a classification prediction. The upper panel illustrates how concepts are formed from
 197 features selected from a diverse training set and then used to analyze other images.

200 3.3 CONCEPTUAL ARCHETYPE DECOMPOSITION

202 3.3.1 CONCEPT EXTRACTION AND INTERPRETATION

204 Although the CRAFT method proposes extracting concepts through NMF (Lee & Seung, 1999) to enhance
 205 model transparency, its biggest challenge lies in concept interpretability. Because the concept dictionary
 206 matrix W generated during NMF decomposition is an optimization artifact, it lacks inherent meaning or
 207 intuitive interpretation. To understand the meaning of a specific concept, it is often necessary to sample
 208 activation values and extract corresponding images for visualization. However, activation values alone do not
 209 directly reflect the specific content of the concept. For example, there may be images with high activation
 210 values that do not exclusively represent a specific concept. For example, suppose we sample three images
 211 with activation values of 1.6, 1.1, and 0.5, representing varying degrees of activation for the same concept.
 212 However, this simple sorting of activation values is insufficient to provide a clear conceptual interpretation, as
 213 high activation values do not always imply that the image’s content fully aligns with the extracted concept.
 214 For example, an image with an activation value of 1.6 may contain a mixture of multiple concepts, rather
 215 than simply the salient features of that concept. Therefore, this approach fails to clearly define the specific
 boundaries and meaning of a concept, and the activation threshold for sampling lacks standardization and
 controllability. This makes concept interpretability ambiguous and unreliable.

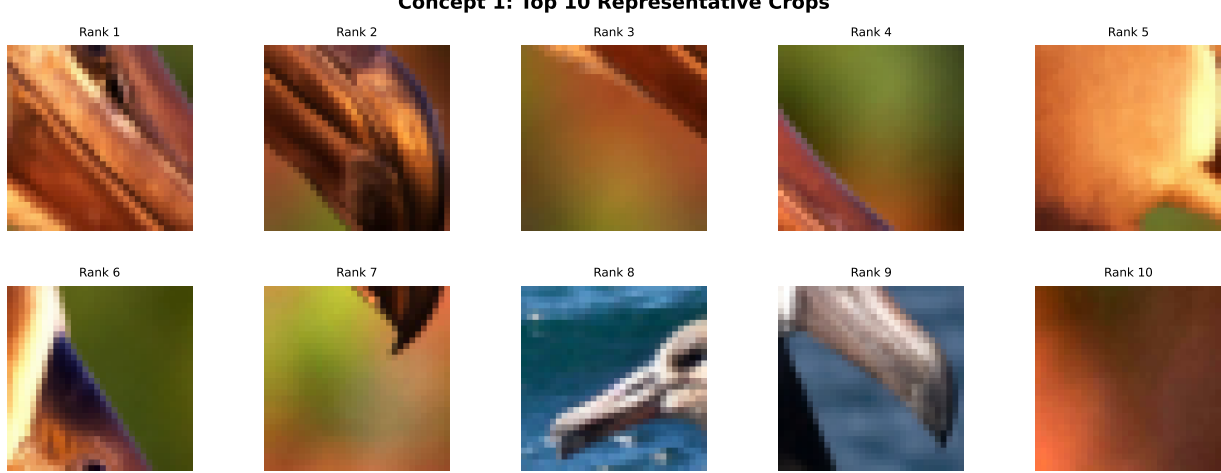


Figure 2: Visualization of conceptual archetype decomposition on CUB dataset: example 1

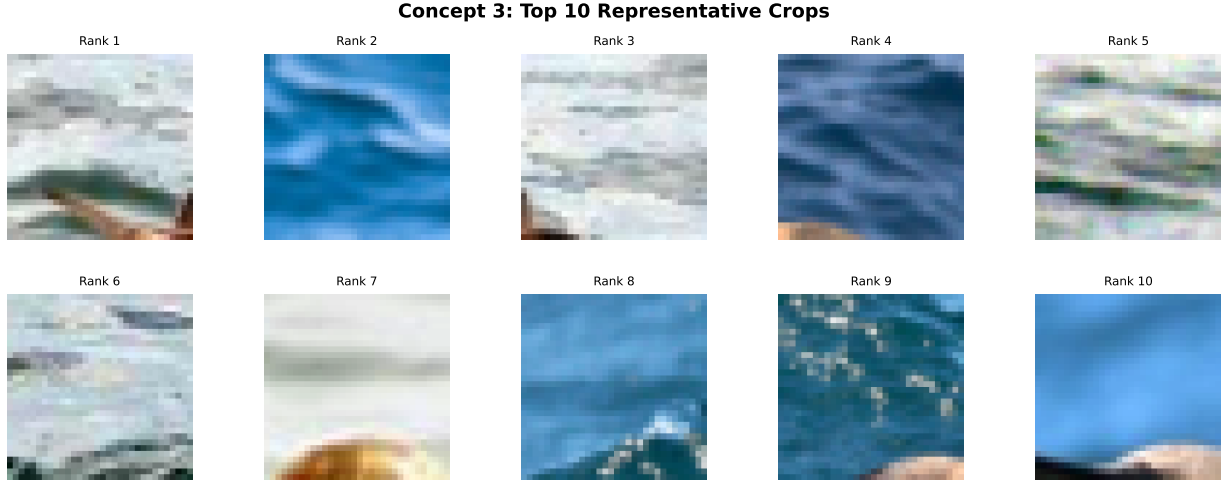


Figure 3: Visualization of conceptual archetype decomposition on CUB dataset: example 2

256 In this section, to provide a traceable intrinsic explanation for the concepts extracted during matrix decom-
 257 position and to establish connections between test and training samples, as shown in Figure 1, we represent
 258 the concept reconstruction process as $A \approx A^\top C^\top B$ and call this method CAD, where A is the activation ma-
 259 trix containing the intermediate layer features of the sample and used to represent the sample, $C \in \mathbb{R}^{k \times nwh}$
 260 is the concept index matrix, and $B \in \mathbb{R}^{nwh \times k}$ is the concept reconstruction matrix. Specifically, assuming
 261 that the activation matrix we extract from the intermediate layer of the neural network is $A \in \mathbb{R}^{nwh \times c}$, we
 262 hope to decompose the concept represented by z into a linear combination of the activation matrix A and the
 263 concept index matrix C , in the form $z = A^\top C^\top$. To ensure that the concepts extracted during training
 264 can be traced back to the training samples, we need to add a restriction $\forall i, \sum_{j=1}^{nwh} C_{ij} = 1$ to the concept
 265 index matrix C . To ensure that this restriction is strictly true, we perform softmax normalization on the
 266 second dimension of the C matrix in each calculation so that the sum of each column in the matrix is 1:
 267
 268

$$C_{ij} = \frac{e^{c_{ij}}}{\sum_{j=1}^{nwh} e^{c_{ij}}} \quad (2)$$

This means that for the elements C_{ij} in the concept index matrix C , they play a one-to-one corresponding role with the feature activation A of the intermediate layer of the sample in the construction of the concept z . Therefore, our concepts are completely obtained by linear combinations of samples, and any concept can find its constituent feature activations and their weights. At the same time, because the feature activations are spatially associated with the original features (Selvaraju et al., 2017), we can find the image location information of the explanation and use it as the explanation. This also means that since z is strictly composed of the activation matrix A and the concept index matrix C , when we need to get the explanation of the concept, we can directly find the corresponding activation matrix composition through C and find the samples behind it as the explanation. CRAFT needs to use samples for sampling to obtain samples with higher activation values as the explanation of the concept, but this also means that this explanation of the concept is not absolutely accurate. In Figure 2 and 3, we visualize the index sources of Concept 1, which are extracted from different training set image crops, ordered by their index values C_{ij} from high to low.

3.3.2 BUILDING ASSOCIATIONS BETWEEN CONCEPTS AND ORIGINAL SAMPLES

In addition to the concept index matrix C , we also introduce a concept reconstruction matrix B , which is used to reconstruct concepts, with $\forall i, \sum_{j=1}^k B_{ij} = 1$. B reconstructs samples by controlling the activation level of each concept. Specifically, B indicates which concepts comprise the sample. We use the same operations as for the concept index matrix C . Figure 4 shows the training process of our CAD method.

Here we want to compare the matrix B with the activation matrix U in CRAFT. The B matrix has two obvious advantages: 1. Unified dimensionality. In the demonstration U , the activation values of different concepts cannot be compared. For example, the value of a certain feature dimension U is between 0-5, while another may be between 0-1. The different dimensions also mean that we cannot determine the activation of a concept by the value of U . 2. U represents the activation value of the concept, while B represents "composition". Because the sum of the second dimension in the matrix B is constrained to be fixed at 1, we can ensure that the reconstructed activation value is completely composed of the concepts in Z , while activation values can only be compared with concepts. In summary, the goal of our CAD optimization is:

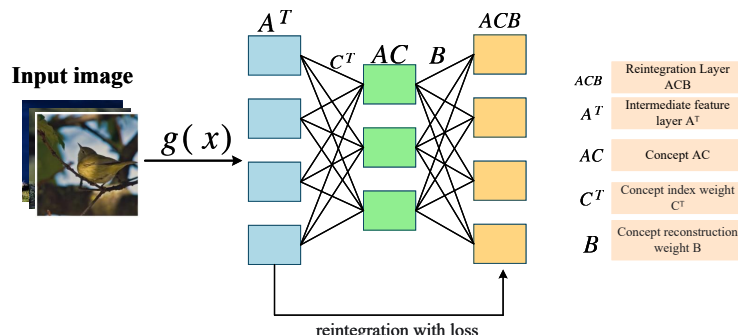


Figure 4: The architecture of our proposed Conceptual Archetype Decomposition (CAD) method.

$$\hat{B}, \hat{C} = \min_{\hat{B}, \hat{C}} \|\hat{A} - \hat{A}^\top \hat{C}^\top \hat{B}\| \quad \text{s.t. } \forall i, \sum_{j=1}^{nwh} \hat{C}_{ij} = 1, \forall i, \sum_{j=1}^k \hat{B}_{ij} = 1 \quad (3)$$

Next, we need to analyze the properties of CAD. CAD satisfies nested double-convex combination, which is easy to prove:

$$A_i \approx \sum_{j=1}^k B_{ij} Z_j = \sum_{j=1}^k B_{ij} \left(\sum_{\ell=1}^{nwh} C_{j\ell} A_\ell \right) = \sum_{\ell=1}^{nwh} \left(\sum_{j=1}^k C_{j\ell} B_{ij} \right) A_\ell. \quad (4)$$

That is,

$$A^\top C^\top B \subseteq \text{conv}(Z) \subseteq \text{conv}(A) \quad (5)$$

324 Where $\text{cone}(X)$ represents the convex hull of the original data. For ease of understanding, we give the
 325 definition of the convex hull here:
 326

$$327 \quad \text{conv}(X) := \left\{ \sum_{i=1}^n \alpha_i x_i \mid \alpha_i \geq 0, \sum_{i=1}^n \alpha_i = 1 \right\} \quad (6)$$

331 Here, $X = \{x_1, x_2, \dots, x_n\} \subset \mathbb{R}^d$. This property also means that any reconstruction can be fully indexed.
 332 However, PCA and CRAFT often project points outside the data convex hull, resulting in unrealistic and
 333 difficult-to-interpret combinations. This can easily lead to interpretation crises in scenarios requiring strict
 334 interpretability. Our CAD, however, provides a rigorous theoretical guarantee against this.

335 Another important property of CAD is its inherent low-entropy structure. This means that it naturally
 336 produces sparse matrices without the need for a regularized loss function. This avoids the influence of hy-
 337 perparameters when setting regularized loss functions and prevents randomness from affecting the confidence
 338 of the interpretation of the results. This can be explained from the perspective of the degrees of freedom of
 339 the matrices. Due to the constraint that the sum is unity, the degrees of freedom of the B matrix are Δ^{k-1} ,
 340 and the degrees of freedom of the a matrix are Δ^{nwh-1} . This is then simply proved using Carathéodory's
 341 theorem (Carathéodory, 1907). In practice, data distributions often approximate the ground-dimensional
 342 manifold, so the sparsity can be even greater than the upper bound proven by Carathéodory's theorem.

343 CAD also has a very advantageous property: **archetypes converge to the extreme points of the**
 344 **convex hull of the data.** Intuitively, a pole cannot be written as a convex combination of two other points
 345 in the convex hull. That is, in convex analysis, a point $x \in \mathcal{C} = \text{conv}(X)$ is a pole if and only if:

$$347 \quad x \neq \lambda x' + (1 - \lambda)x'', \quad \forall x', x'' \in \mathcal{C} \setminus \{x\}, \lambda \in (0, 1) \quad (7)$$

349 This also means that the decomposition of concepts will select representative samples, and when recon-
 350 structing samples, representative concepts will be selected. Concepts and reconstructed samples have nat-
 351 ural atomicity, which can be easily proved using the Cutler & Breiman theorem Cutler & Breiman (1994)
 352 combined with the convex hull property.

353 Finally, in the interaction phase, if we want to obtain a unified conceptual explanation, we only need to fix Z ,
 354 which is $A^\top C^\top$ during training, and use Eq. 3 to optimize the new B matrix to obtain a unified explanation.

357 4 EXPERIMENT

359 4.1 EXPERIMENTAL SETUP

361 In this paper, we design and implement multiple experiments to validate the effectiveness and superiority of
 362 the proposed Conceptual Archetype Decomposition (CAD) method. We use two widely adopted benchmark
 363 datasets in visual tasks: CUB (Wah et al., 2011) and ImageNet (Deng et al., 2009), and select two common
 364 deep learning models as backbones: NF_ResNet50 (Brock et al., 2021) and VIT-B/32(Dosovitskiy et al.,
 365 2021). Specifically, the CUB dataset contains images of 200 bird species, providing rich fine-grained label
 366 information, making it suitable for testing the model's performance in fine-grained object classification. The
 367 ImageNet dataset, with 1,000 object categories, has a large-scale data set, making it ideal for evaluating
 368 the model's robustness and generalization ability in large-scale visual classification tasks. To comprehen-
 369 sively assess our CAD method, we choose two competitive baseline methods: CRAFT (Fel et al., 2023)
 370 and PCA (Jolliffe, 1986). The CRAFT method, which extracts concepts based on Non-negative Matrix
 371 Factorization, serves as a direct comparison to our method, while PCA, as a classic dimensionality reduction
 372 method, is used as another baseline to demonstrate the differences in model interpretability and performance
 373 between various concept extraction methods.

374 4.2 EXPERIMENT 1: VALIDATION OF CONCEPT RECONSTRUCTION ERROR

376 To evaluate the reconstruction error of concepts on both the training and test sets, we propose a val-
 377 idation method based on Mean Squared Error (MSE). A smaller MSE indicates that the reconstructed
 features closely match the original features. The results of this experiment are presented in Table 1. This

experiment probes whether CAD’s convex-combination design— $\hat{A} = A^\top C^\top B$ with per-column simplex constraints on C and B —translates into *in-distribution* reconstructions at test time. The key signal is the generalization gap $\Delta = \text{MSE}_{\text{test}} - \text{MSE}_{\text{train}}$ (the “Variation” column), not the raw training MSE whose magnitude is confounded by backbone feature scales. Across all datasets/backbones, CAD yields gaps that are *approximately* $5.9 \times -12.9 \times$ smaller than CRAFT and $3.3 \times -12.8 \times$ smaller than PCA (e.g., CUB/NF-ResNet50: 24.73 vs. 156.35/170.78; CUB/ViT-B/32: 0.26 vs. 1.54/0.87; ImageNet/NF-ResNet50: 0.08 vs. 1.03/1.02; ImageNet/ViT-B/32: 0.12 vs. 1.35/0.79). This pattern matches the method’s inductive bias: since $\hat{A} \in \text{conv}(A)$, CAD reconstructs test activations as convex mixtures of training activations and avoids *off-hull* extrapolation. In contrast, dictionary–coefficient factorizations (e.g., NMF-style UW in CRAFT) can aggressively minimize train error yet reconstruct test features outside the training hull, inflating Δ despite tiny training MSE (e.g., CUB/NF-ResNet50: 1.87 → 158.21). Put differently, CAD trades a bit of training fit for *distribution-matched* test reconstructions—a bias–variance choice enforced by the simplex/low-entropy structure of B and C , which acts as an implicit regularizer. The smallest gaps appear on the larger ImageNet and the stronger ViT-B/32 backbone, suggesting that the convex-hull constraint scales favorably as the feature geometry becomes richer (consistent with archetypes concentrating near extreme points of $\text{conv}(A)$). Finally, these results empirically corroborate the critique of cropping-based decompositions: when training/decomposition inputs are mismatched (sub-regions vs. full images), test reconstructions drift; CAD’s full-image mapping maintains train/test alignment.

Table 1: Validation table of Concept Reconstruction Error (Train vs. Test). We report mean \pm std and *Variation* = Test – Train. The smallest *Variation* per dataset is bolded.

Model		CUB / NF-ResNet50			CUB / ViT-B/32		
Variant	Dataset	Train	Test	Variation	Train	Test	Variation
Ours	CUB	86.74 ± 22.37	111.48 ± 24.03	24.73	1.14 ± 0.17	1.40 ± 0.16	0.26
CRAFT	CUB	1.87 ± 0.46	158.21 ± 36.66	156.35	1.01 ± 0.06	2.55 ± 0.09	1.54
PCA	CUB	5.56 ± 1.10	176.33 ± 40.48	170.78	0.93 ± 0.30	1.80 ± 0.21	0.87
Model		ImageNet / NF-ResNet50			ImageNet / ViT-B/32		
Variant	Dataset	Train	Test	Variation	Train	Test	Variation
Ours	ImageNet	0.89 ± 0.18	0.97 ± 0.19	0.08	1.46 ± 0.16	1.58 ± 0.16	0.12
CRAFT	ImageNet	0.10 ± 0.02	1.14 ± 0.19	1.03	1.14 ± 0.07	2.49 ± 0.10	1.35
PCA	ImageNet	0.19 ± 0.03	1.20 ± 0.20	1.02	1.06 ± 0.29	1.85 ± 0.20	0.79

4.3 EXPERIMENT 2: VALIDATION OF CONCEPT RECONSTRUCTION CLASSIFICATION ACCURACY

This evaluation asks a stronger question than Exp. 1: not only must the reconstruction be close to the original features, it must also be *decision preserving*. We therefore classify *only from reconstructed features* and sweep the number of concepts k (Table 2, Fig. 5). Two signals matter: (i) the *level* of accuracy after reconstruction and (ii) its *stability* as k varies.

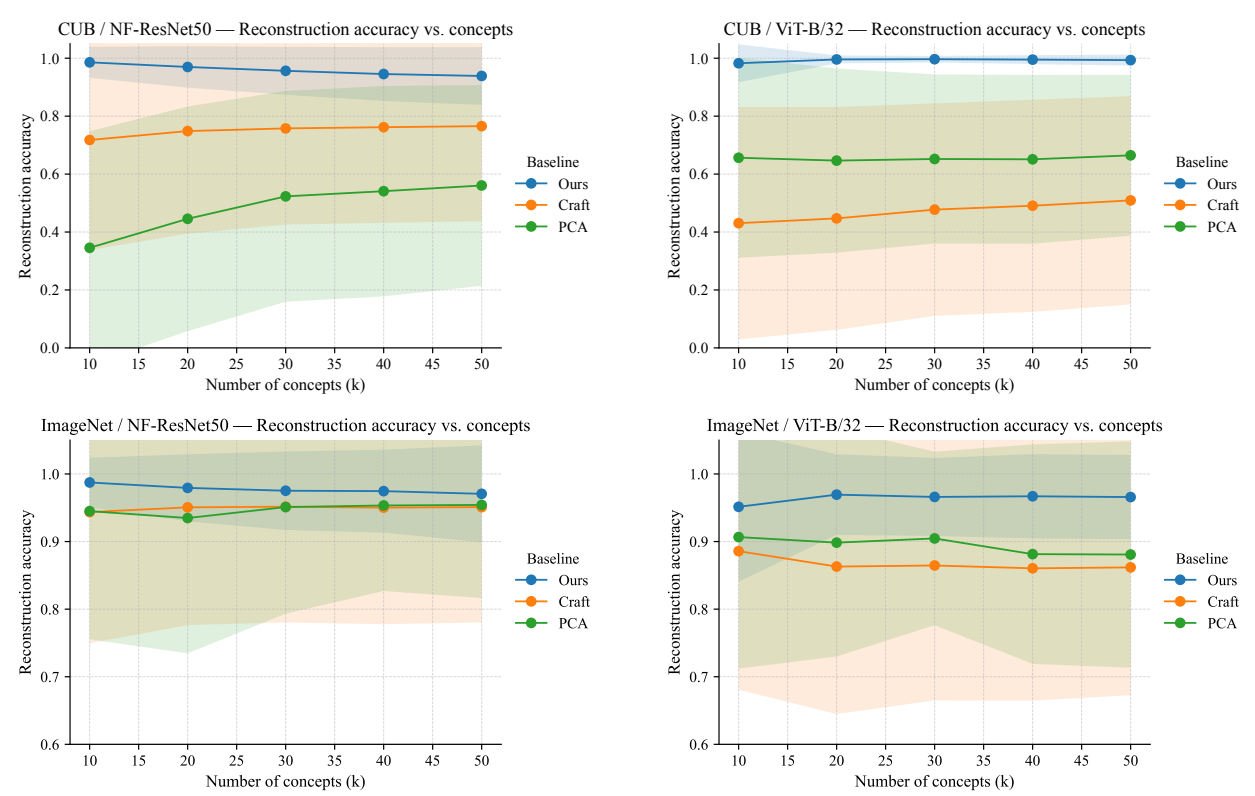
Level. CAD attains near-ceiling accuracy across datasets/backbones (typically 99%–100%), while CRAFT/PCA trail substantially—by +30–65 points on CUB and +5–13 points on ImageNet. This aligns with CAD’s convex-hull bias: the mapping $\hat{A} \in \text{conv}(A)$ keeps test features inside the training support, so a Lipschitz classifier (e.g., a linear head) experiences at most a bounded logit perturbation proportional to $\|A - \hat{A}\|$; hence decision regions and margins are largely preserved. In contrast, CRAFT’s free dictionary and PCA’s global subspace can push reconstructions *off-hull*, which degrades separability even when training error is small (See §4.2).

Stability. CAD’s mean \pm std bands are narrow and essentially *flat* in k ; CRAFT/PCA exhibit large dispersion (std up to ≈ 40 on CUB) and non-monotone slopes, indicating a “ k -lottery” effect where adding concepts changes the factorization in ways that disrupt the classifier. By constraining B, C to simplices, CAD enforces sparse, low-entropy mixtures that vary smoothly with k , acting as an implicit regularizer that keeps decision geometry consistent.

Backbone/dataset trends. Gaps shrink on ImageNet and ViT-B/32 because the base representations are already highly linearly separable; nevertheless CAD retains a consistent edge and the tightest variability, suggesting that the convex-combination mechanism scales favorably as the feature geometry becomes richer. On CUB, where features are more brittle and class margins are thinner, CAD’s no-extrapolation property is most beneficial, yielding the largest accuracy gains and the smallest variance.

432 Table 2: Validation of concept reconstruction classification accuracy (%). We report mean \pm std across
 433 seeds; higher is better. Best per column is in **bold**.

#Concepts k	CUB / NF-ResNet50			CUB / ViT-B/32			ImageNet / NF-ResNet50			ImageNet / ViT-B/32		
	Ours	CRAFT	PCA	Ours	CRAFT	PCA	Ours	CRAFT	PCA	Ours	CRAFT	PCA
10	99.5 ± 5.4	71.8 ± 38.0	34.5 ± 40.3	99.6 ± 2.5	43.1 ± 40.1	65.6 ± 34.5	99.9 ± 0.8	94.4 ± 19.4	95.0 ± 19.0	97.6 ± 8.8	88.6 ± 20.5	90.7 ± 19.5
	99.5 ± 4.3	74.9 ± 35.4	44.6 ± 38.8	99.8 ± 1.8	44.7 ± 38.5	64.7 ± 31.8	99.9 ± 0.9	95.1 ± 17.4	93.5 ± 20.0	98.5 ± 5.1	86.3 ± 21.8	89.8 ± 16.8
20	99.4 ± 4.9	75.8 ± 33.2	52.3 ± 36.4	100.0 ± 0.3	47.7 ± 36.7	65.2 ± 29.2	99.8 ± 1.0	95.2 ± 17.1	95.1 ± 15.8	99.0 ± 3.9	86.5 ± 20.0	90.5 ± 12.8
	99.4 ± 5.4	76.2 ± 33.0	54.1 ± 36.3	99.9 ± 0.5	49.1 ± 36.6	65.1 ± 29.1	99.8 ± 1.3	95.0 ± 17.2	95.3 ± 12.7	99.3 ± 1.9	86.0 ± 19.6	88.1 ± 16.2
30	99.3 ± 5.3	76.6 ± 32.8	56.1 ± 34.6	100.0 ± 0.0	50.9 ± 36.0	66.5 ± 36.0	99.6 ± 1.2	95.1 ± 17.1	95.4 ± 13.8	99.3 ± 2.9	86.2 ± 18.9	88.1 ± 16.7



471 Figure 5: Validation chart of concept reconstruction classification accuracy.

474 5 CONCLUSION

477 This paper presents a novel concept extraction method—Conceptual Archetype Decomposition
 478 (CAD)—designed to enhance the interpretability and robustness of concept-based deep learning models.
 479 By introducing a concept index matrix and a concept reconstruction matrix, CAD ensures a direct association
 480 between the extracted concepts and the training samples, overcoming the limitations of existing methods
 481 (such as CRAFT and PCA) in terms of concept interpretability and generalization ability. Our experimental
 482 results demonstrate the effectiveness and superiority of CAD on several benchmark datasets, including CUB
 483 and ImageNet. Overall, CAD not only provides more intuitive and reliable concept representations for model
 484 interpretability, but also shows stronger performance and robustness in multi-class classification tasks. Our
 485 method offers new insights for research on explainable deep learning models, with significant theoretical
 486 value and application potential, particularly in high-risk fields such as healthcare and autonomous driving,
 487 where enhancing the transparency and safety of model decision-making processes is of critical importance.

486 ETHICS STATEMENT
487

488 We have read and will adhere to the ICLR Code of Ethics. This work uses only public data, involves no
489 human subjects or personally identifiable information, and therefore does not require IRB review. Results
490 are reported for research purposes only; we release anonymized code/configurations to support verification,
491 and will disclose any funding sources and potential conflicts of interest upon acceptance.

492
493 REPRODUCIBILITY STATEMENT
494

495 To support reproducibility, we release an anonymized repository with all experiment details including training/
496 evaluation scripts, default hyperparameters, configuration files, and software/hardware environment.
497

498 REFERENCES
499

500 Andy Brock, Soham De, Samuel L Smith, and Karen Simonyan. High-performance large-scale image recog-
501 nition without normalization. In *International conference on machine learning*, pp. 1059–1071. PMLR,
502 2021.

503 Constantin Carathéodory. Über den variabilitätsbereich der koeffizienten von potenzreihen, die gegebene
504 werte nicht annehmen. *Mathematische Annalen*, 64(1):95–115, 1907.

505 Maelenn Corfmat, Joé T Martineau, and Catherine Régis. High-reward, high-risk technologies? an ethical
506 and legal account of ai development in healthcare. *BMC medical ethics*, 26(1):4, 2025.

507 Adele Cutler and Leo Breiman. Archetypal analysis. *Technometrics*, 36(4):338–347, 1994.

508 Jia Deng, Wei Dong, Richard Socher, Li-Jia Li, Kai Li, and Li Fei-Fei. Imagenet: A large-scale hierarchical
509 image database. In *2009 IEEE conference on computer vision and pattern recognition*, pp. 248–255. Ieee,
510 2009.

511 Alexey Dosovitskiy, Lucas Beyer, Alexander Kolesnikov, Dirk Weissenborn, Xiaohua Zhai, Thomas Unterthiner,
512 Mostafa Dehghani, Matthias Minderer, Georg Heigold, Sylvain Gelly, et al. An image is worth
513 16x16 words: Transformers for image recognition at scale. In *International Conference on Learning Rep-
514 resentations*, 2021.

515 Thomas Fel, Agustin Picard, Louis Bethune, Thibaut Boissin, David Vigouroux, Julien Colin, Rémi Cadène,
516 and Thomas Serre. Craft: Concept recursive activation factorization for explainability. In *Proceedings of
517 the IEEE/CVF Conference on Computer Vision and Pattern Recognition*, pp. 2711–2721, 2023.

518 Ian Goodfellow, Yoshua Bengio, and Aaron Courville. *Deep learning*, volume 1. MIT press Cambridge, 2016.

519 Ian T Jolliffe. *Principal Component Analysis*. Springer, 1986.

520 Been Kim, Martin Wattenberg, Justin Gilmer, Carrie Cai, James Wexler, Fernanda Viegas, et al. Inter-
521 pretability beyond feature attribution: Quantitative testing with concept activation vectors (tcav). In
522 *International conference on machine learning*, pp. 2668–2677. PMLR, 2018.

523 Pang Wei Koh, Thao Nguyen, Yew Siang Tang, Stephen Mussmann, Everett Pierson, Been Kim, and Percy
524 Liang. Concept bottleneck models. In *Proceedings of the 37th International Conference on Machine
525 Learning (ICML)*, volume 119, pp. 5338–5348. PMLR, 2020.

526 Neehar Kondapaneni, Oisin Mac Aodha, and Pietro Perona. Representational similarity via interpretable
527 visual concepts. *arXiv preprint arXiv:2503.15699*, 2025.

528 Daniel D Lee and H Sebastian Seung. Learning the parts of objects by non-negative matrix factorization.
529 *nature*, 401(6755):788–791, 1999.

530 Jae Hee Lee, Georgii Mikriukov, Gesina Schwalbe, Stefan Wermter, and Diedrich Wolter. Concept-based
531 explanations in computer vision: Where are we and where could we go? In *European Conference on
532 Computer Vision*, pp. 266–287. Springer, 2024.

540 Scott M Lundberg and Su-In Lee. A unified approach to interpreting model predictions. *Advances in neural*
 541 *information processing systems*, 30, 2017.

542

543 Marco Tulio Ribeiro, Sameer Singh, and Carlos Guestrin. " why should i trust you?" explaining the predictions
 544 of any classifier. In *Proceedings of the 22nd ACM SIGKDD international conference on knowledge discovery*
 545 *and data mining*, pp. 1135–1144, 2016.

546

547 Ramprasaath R Selvaraju, Michael Cogswell, Abhishek Das, Ramakrishna Vedantam, Devi Parikh, and
 548 Dhruv Batra. Grad-cam: Visual explanations from deep networks via gradient-based localization. In
 549 *Proceedings of the IEEE international conference on computer vision*, pp. 618–626, 2017.

550

551 Harshay Shah, Sung Min Park, Andrew Ilyas, and Aleksander Madry. Modeldiff: A framework for comparing
 552 learning algorithms. In *International Conference on Machine Learning*, pp. 30646–30688. PMLR, 2023.

553

554 Mukund Sundararajan, Ankur Taly, and Qiqi Yan. Axiomatic attribution for deep networks. In *International*
 555 *conference on machine learning*, pp. 3319–3328. PMLR, 2017.

556

557 Catherine Wah, Steve Branson, Peter Welinder, Pietro Perona, and Serge Belongie. The Caltech-UCSD
 558 Birds-200-2011 Dataset. Technical Report CNS-TR-2011-001, California Institute of Technology, 2011.

559

560 Yue Wang and Sai Ho Chung. Artificial intelligence in safety-critical systems: a systematic review. *Industrial*
 561 *Management & Data Systems*, 122(2):442–470, 2022.

562

563 Zhiyu Zhu, Huaming Chen, Jiayu Zhang, Xinyi Wang, Zhibo Jin, Minhui Xue, Dongxiao Zhu, and Kim-
 564 Kwang Raymond Choo. Mfaba: A more faithful and accelerated boundary-based attribution method for
 565 deep neural networks. In *Proceedings of the AAAI Conference on Artificial Intelligence*, volume 38, pp.
 566 17228–17236, 2024.

567

568

569

570

571

572

573

574

575

576

577

578

579

580

581

582

583

584

585

586

587

588

589

590

591

592

593

594 **LLM USAGE DISCLOSURE**
595596 We used large language models (OpenAI GPT-4o and GPT-5) as auxiliary tools for grammar checking and
597 language polishing of the manuscript. These models were not involved in research ideation, experimental
598 design, implementation, or analysis. The authors take full responsibility for all content.
599

600

601

602

603

604

605

606

607

608

609

610

611

612

613

614

615

616

617

618

619

620

621

622

623

624

625

626

627

628

629

630

631

632

633

634

635

636

637

638

639

640

641

642

643

644

645

646

647